Optoelectronic Properties and Applications of Rare-Earth-Doped GaN

A.J. Steckl and J.M. Zavada

Introduction

As discussed in the accompanying articles in this issue of *MRS Bulletin*, the optical properties of rare-earth (RE) elements have led to many important photonic applications, including solid-state lasers, components for telecommunications (optical-fiber amplifiers, fiber lasers), optical storage devices, and displays. In most of these applications, the host materials for the RE elements are various forms of oxide and nonoxide glasses. The emission can occur at visible or infrared (IR) wavelengths, depending on the electronic transitions of the selected RE element and the excitation mechanism. Until recently, the study of semiconductors doped with RE elements such as Pr and Er has concentrated primarily on the lowest excited state as an optically active transition. The presence of transitions at IR wavelengths (1.3 and 1.54 μm) that are coincident with minima in the optical dispersion and the loss of silica-based glass fibers utilized in telecommunications, combined with the prospect of integration with semiconductor device technology, has sparked considerable interest.

The status and prospects of obtaining stimulated emission in Si:Er are reviewed by Gregorkiewicz and Langer in this issue and by Coffa et al.[1] in a previous *MRS Bulletin* issue. While great progress is being made in enhancing the emission intensity of Er-doped Si, it still experiences significant loss in luminescence efficiency at room temperature, as compared with low temperatures. This thermal quenching was shown by Favennec et al.[2] to decrease with the bandgap energy of the semiconductor. Hence wide-bandgap semiconductors (WBGSs) are attractive candidates for investigation as hosts for RE doping.

Figure 1 shows the bandgap of many semiconductors important for optoelectronics as a function of lattice constant in the basal plane of their crystal structure.[3–5] The most common crystal structures are the diamond cubic structure for the elemental semiconductors (C, Si, Ge) and zinc-blende cubic and hexagonal (wurtzite) structures for III-V and II-VI semiconductors. The cubic form of the III-N compounds is metastable and is found under certain conditions of growth on cubic substrates. The bandgap energy values of these cubic III-N semiconductors are not as "time-tested" as those of their wurtzite counterparts. SiC is a special case, forming a large variety of polytypes, with the cubic 3C and hexagonal 6H and 4H polytypes being the most heavily investigated. For the hexagonal materials, the basal-plane lattice constant is used in Figure 1. The semiconductors labeled in italics have an indirect bandgap, which results in significantly less-efficient light emission than direct bandgap semiconductors. The color scheme in Figure 1 is intended to provide only a very approximate idea of the colors of the visible spectrum associated with band-to-band transitions in the various semiconductors included in the graph.

An arbitrary but accepted definition of the boundary separating WBGSs from other semiconductors is a bandgap energy of 2 eV. With the exception of some

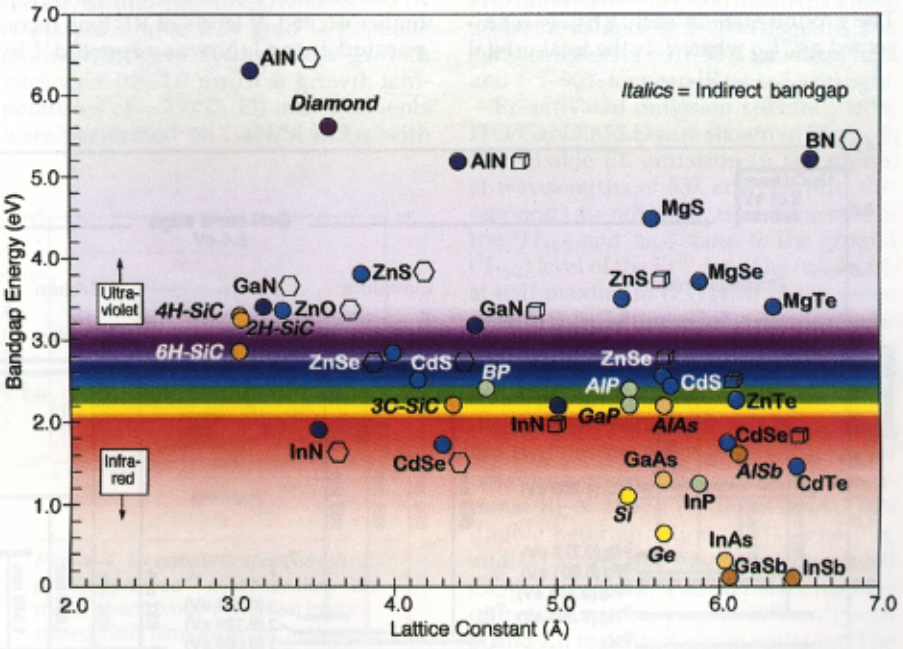

Figure 1. Bandgap energy and lattice constant of many semiconductors important for optoelectronics. In the case of SiC and III-N compounds, both cubic (zinc-blende) and hexagonal crystal polytypes are shown. For the hexagonal materials, the basal-plane lattice constant is used. The colored regions approximate the band-to-band photoemission corresponding to the bandgap energy.

of the II-VI compound semiconductors, the advantages of WBGSs over smaller-gap semiconductors and glasses include greater chemical stability, carrier generation (to excite the RE ions), and physical stability over a wide temperature range. The III-N semiconducting compounds are of particular interest because of their direct bandgap and high level of optical activity[6] even under conditions of high defect density, which would quench emission in other smaller-gap III-V and in most II-VI compounds. Light-emitting diodes (LEDs) and laser diodes fabricated using GaN-based structures[7,8] have recently become commercially available, and their utilization is rapidly increasing. In this article, we review the recent developments with RE doping of GaN for optoelectronic applications.

Rare-Earth Doping

RE-activated photoluminescence (PL), cathodoluminescence (CL), and most important, electroluminescence (EL) from device (ELD) structures have been observed in GaN doped with several RE elements. In Figure 2, we show simplified energy diagrams of $^{59}Pr_{141}$, $^{63}Eu_{152}$, $^{68}Er_{167}$, and $^{69}Tm_{169}$. The electronic structure of each trivalent RE element (RE^{3+}) consists of a partially filled $4f$ subshell and completely filled outer $5s^2$ and $5p^6$ subshells. With increasing nuclear charge, electrons enter into the underlying $4f$ subshell rather than the external $5d$ subshell. The ground state of each RE^{3+} is represented as $^{m}L_J$, where L is the total orbital angular momentum, J is the total angular momentum, and m is the multiplicity of terms in the atomic configuration. Since the filled $5s^2$ and $5p^6$ subshells screen the $4f$ electrons, the RE elements have very similar optical properties in various host materials.

Also indicated in Figure 2 are the conduction-band edge of GaN and the photon energies of He-Cd and Ar lasers, which are widely utilized for above- and below-bandgap PL characterization of RE-doped GaN. The wavelengths of the dominant EL and/or PL emission lines observed to date from these materials are indicated in each diagram, along with the identified electronic transitions. The energy of the majority of RE levels shown is the experimental value for GaN:RE, based on the corresponding emission wavelength, with the few remaining values (in italics) being based[9] on the properties of RE-doped crystals.

Wilson et al.[10] were the first to observe strong IR photoluminescence, centered at 1.54 μm, from Er-implanted GaN thin films. As seen in Figure 2, this emission corresponds to radiative transitions between the first excited state ($^4I_{13/2}$) and the ground ($^4I_{15/2}$) levels of the Er^{3+} ion. Coimplantation with O and furnace annealing were needed to achieve the strong luminescence. Several other research groups[11–13] have also used ion implantation to dope GaN films with Er.

The discovery of visible emission from higher excited $4f$ levels of RE ions incorporated into GaN was reported[14] by Steckl and Birkhahn. They described Er *in situ* incorporation during GaN growth by molecular-beam epitaxy (MBE) on sapphire. The resulting GaN:Er films exhibited intense green PL from the $^2H_{11/2}$ and $^4S_{3/2}$ states. The emission was visible with the naked eye at room temperature. This was followed in quick succession by reports of visible PL from GaN:Er on Si substrates,[15] green EL from GaN:Er devices using aluminum[16] and indium-tin oxide[17] (ITO) contacts, red EL from Pr-doped[18] and Eu-doped[19] devices, blue EL from GaN:Tm devices,[20] and blue-green ("aqua") EL from Er- and Tm-codoped GaN devices.[21] The three primary colors and one mixed color emitted from these RE-doped GaN ELDs are seen in the photograph on the cover of this issue. The $4f$ radiative transitions resulting in visible and IR emission for GaN doped with these RE ions are indicated in Figure 2. Visible CL was also recently reported[22] for GaN films implanted with Dy, Er, and Tm.

As just discussed, one of the critical issues in RE-doped semiconductors is the thermal quenching of the luminescence near room temperature. The second major issue in the RE doping of GaN is the ability to incorporate a significant concentration of RE ions without precipitation and without quenching the PL or EL intensity. Introduction of RE ions by ion implantation has the advantage of being able to produce a concentration level beyond the thermal equilibrium level. The implantation approach has been used for

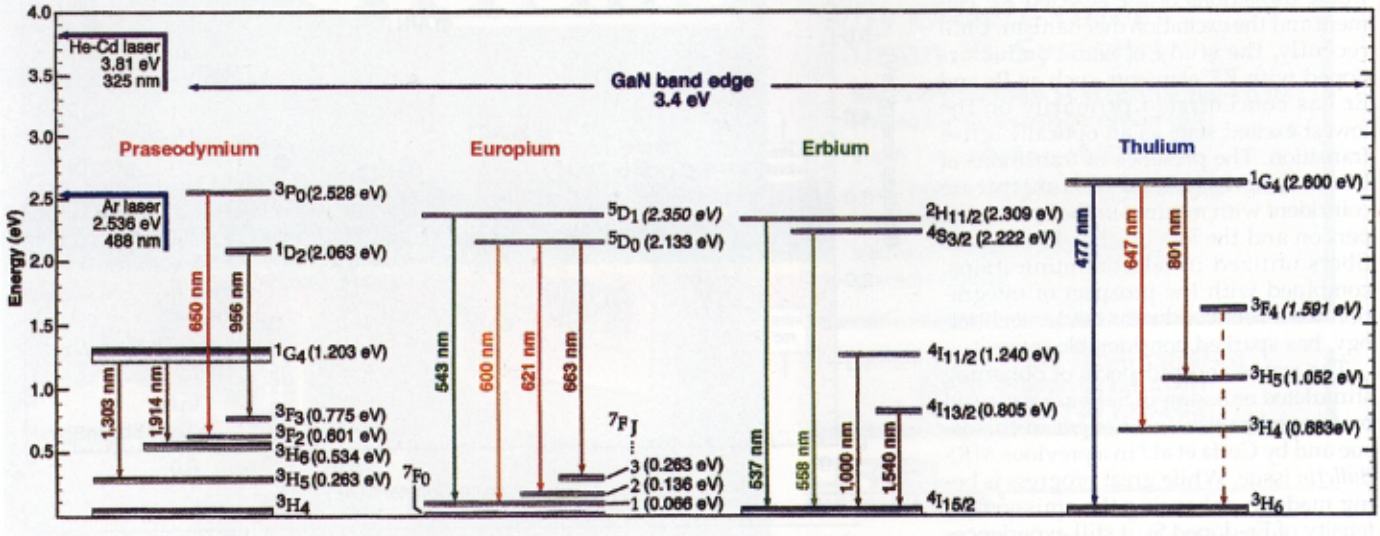

Figure 2. Simplified energy diagrams of the 4f levels of selected rare-earth (RE) ions (Pr, Eu, Er, and Tm) in GaN. The GaN conduction-band edge and the photon energies of He-Cd and Ar lasers, for above and below bandgap photoluminescence (PL), are also shown. The visible and near-infrared (IR) wavelengths of the RE-related electroluminescence (EL) and/or PL emission lines are indicated in each diagram.

Si:Er, where the Er concentration introduced during thin-film growth is usually too low for practical device applications. However, the implantation approach also suffers from several disadvantages. The heavy mass of the RE ions requires high implantation energies, which in turn require thermal annealing for removing the damage and activating the RE ions. At high RE concentrations, the annealing step may actually lead to RE precipitation. Therefore, it is very important to show that both ion implantation and *in situ* incorporation can achieve high RE concentrations and optical activity in GaN.

Thaik et al.[23] have reported on the thermal quenching of 1.5-μm PL for Er-implanted GaN films. GaN films grown on sapphire were coimplanted with Er and O ions. The Er^{3+} emission in the 1.5-μm region under He-Cd laser excitation was measured from 13 to 550 K. As shown in Figure 3a, only minor changes are observed in the PL spectra obtained at 300 and 550 K. The integrated PL intensity is shown in Figure 3b as a function of measurement temperature. The PL intensity at 550 K is reduced by only approximately 10% from its value at 15 K. This is excellent temperature stability over such a wide temperature range and represents the best-reported data from any Er-doped semiconductor, including the very stable SiC:Er system.[24]

Birkhahn et al. have investigated the *in situ* incorporation of Er from a solid source into GaN during growth by MBE on sapphire[25] and on Si[26] substrates. The Er concentration in the GaN film is primarily controlled by the Er cell temperature, with growth temperature and Ga flux also playing important roles. Experiments with GaN:Er on sapphire show that the incorporated Er concentration *and* the PL intensity track very well with the Er cell temperature. No evidence of reaching the solid solubility limit is observed for concentrations up to $3 \times 10^{20}/cm^3$. For GaN growth on Si, even higher Er concentrations have been observed. For example, Figure 4 shows a representative secondary-ion mass spectrometry depth profile of an Er-doped GaN film grown on Si(111). For an Er cell temperature of 1100°C, a very uniform Er concentration of $\sim 6.5 \times 10^{20}/cm^3$ was measured, corresponding to ~0.7 at.% throughout the GaN film. The maximum concentration achieved under the conditions reported was ~5 at.%. These values are surprisingly large and may yet contain some hidden problems, but they clearly indicate that the incorporation and activation of Er and other RE elements into GaN work extremely well.

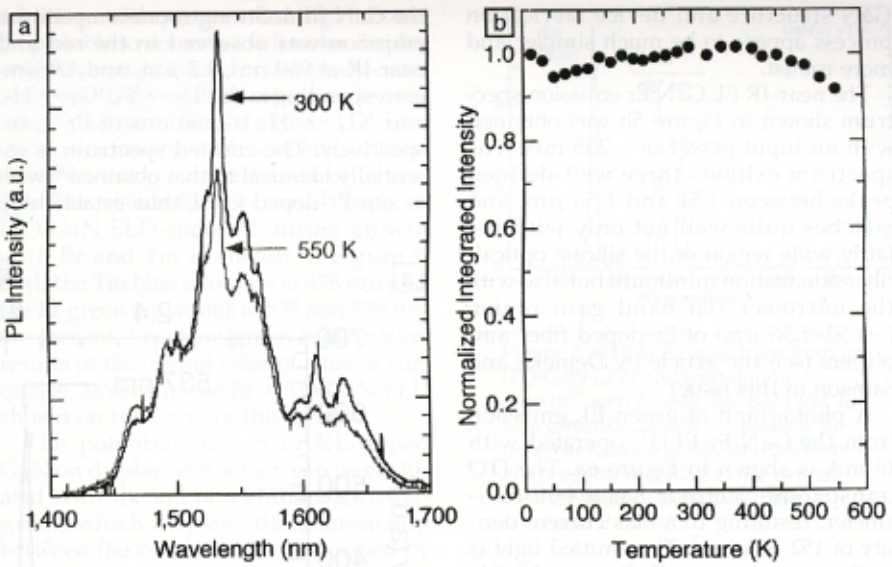

Figure 3. Above-bandgap PL (He-Cd laser at 325 nm) of Er-implanted[23] GaN in the 1.5-μm near-IR region: (a) PL spectra measured at 300 and 550 K; (b) integrated 1.5-μm PL intensity versus temperature from 15 to 550 K.

Visible Light Emission

The results described in this section have been obtained at the University of Cincinnati using *in situ* RE-doped GaN films grown by MBE in a Riber MBE-32 system on Si(111) substrates. Solid sources were employed to supply the Ga and RE (Pr, Eu, Er, and Tm) fluxes, while an SVTA rf-plasma source was used to generate atomic nitrogen. Typical GaN growth rates were 0.8–1.0 μm/h at growth temperatures of ~750°C. EL measurements were performed on GaN/Si ELDs with ITO (90% In-10% Sn) rectifying contacts. The electrical and optical properties of the ITO contact can be tailored[17,27] for high transmission in the visible and/or IR regions and for low sheet resistance by adjusting the film thickness and annealing conditions. Typical properties of ITO films were ~100–500 nm in thickness, a sheet resistance of 5–100 Ω/square, and a transmission of ~70–95% for visible light and ~5–90% for near-IR (at 1–2 μm) light.

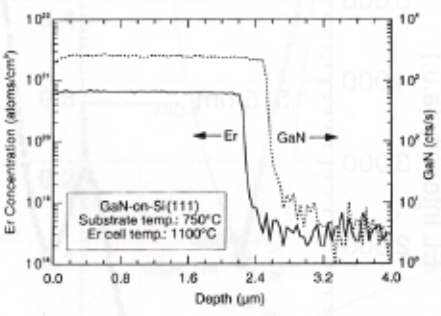

Figure 4. Er concentration depth profile obtained[26] by secondary-ion mass spectrometry from an in situ*-doped GaN film grown by molecular-beam epitaxy on Si(111). The Er cell temperature during growth was 1100°C. A thin (~0.25 μm) undoped GaN "initialization" layer is grown first, followed by a ~2.2-μm Er-doped GaN layer.*

Er-activated emission spectra[17] from ITO/GaN:Er ELDs are shown in Figure 5. The visible EL emission in the green, at wavelengths of 537 and 558 nm, corresponds to radiative transitions from the $^2H_{11/2}$ and $^4S_{3/2}$ states to the ground ($^4I_{15/2}$) level of the Er^{3+} ion. The full width at half maximum (FWHM) of the green lines is 2.5–3.0 nm. Conventional GaN-based green LEDs have an FWHM ranging from 45 to 90 nm, depending on the structure and center wavelength.[7,28] As discussed by Nakamura and Fasol,[7] there are two device-structure approaches for obtaining green LEDs utilizing conventional III-N alloys: (1) an InGaN/AlGaN double heterojunction (DH) structure, and (2) an InGaN single-quantum-well (SQW) structure. The DH structure requires heavy codoping ($\sim 10^{19}$ cm^3) with Si and Zn to achieve green emission. The InGaN SQW structure requires the growth of seven layers, including a 2-nm-thick quantum well. The composition of the SQW determines the emission wavelength. By comparison, the RE-doped

GaN structure and device fabrication process appear to be much simpler and more robust.

The near-IR EL GaN:Er emission spectrum shown in Figure 5b was obtained with an input power of ~235 mW. The spectrum exhibits three well-defined peaks between 1.51 and 1.56 μm, and matches quite well not only with the fairly wide region of the silicate optical-fiber attenuation minimum but also with the narrower flat-band gain region (~1.53–1.56 μm) of Er-doped fiber amplifiers (see the article by Dejneka and Samson in this issue).

A photograph of green EL emission from the GaN:Er ELD[17] operated with 19 mA is shown in Figure 6a. The ITO transparent electrode has a 4-mm diameter, resulting in a bias current density of 152 mA/cm^2. The emitted light is easily seen in a normally lit room. Visible emission from RE ions into GaN has also been accomplished by focused ion-beam (FIB) implantation. FIB technology is a maskless and resistless "direct-write" process that can be applied with great versatility[29] to the fabrication of photonic devices. FIB micro- and nanofabrication (with ion-beam diameters ranging from less than 100 nm to a few microns) can be used to reduce the complexity required of conventional photonic fabrication technology (in particular, lithography, etching, and implantation), which has to satisfy various requirements for different components fabricated on the same substrate. FIB technology can be used to effect local changes in topology (through micromachining) and in electrical and optical properties (through dopant ion implantation and/or mixing). For example, the use of Ga^+ FIB implantation to achieve the micromachining of waveguides and gratings in GaN has recently been reported.[30]

Erbium[31] and praseodymium[32] ion sources suitable for FIB implantation have been developed by combining the RE elements with other metals to form alloys with lower melting points and vapor pressures. Figure 6b shows an image of red PL from a GaN film grown by MBE on sapphire and FIB-implanted[33] with Pr. The implanted pattern is a 141 μm × 141 μm square. The implantation energy and dose are 290 keV and 4.7 × 10^{14} atoms/cm^2, respectively. The sample was annealed at 1050°C for 1 h in Ar after FIB implantation. Under UV excitation from the He-Cd laser, the implanted region emits red light at 650 nm corresponding to the $^3P_0 \rightarrow {}^3F_2$ transition of Pr^{3+}. The unimplanted surrounding area shows the yellow band emission of the GaN film. Strong room-temperature emission was observed in the red and near-IR at 960 nm, 1.3 μm, and 1.9 μm, corresponding to the $^1D_2 \rightarrow {}^3F_3$, $^1G_4 \rightarrow {}^3H_5$, and $^3G_4 \rightarrow {}^3H_6$ transitions of Pr^{3+}, respectively. The emitted spectrum is essentially identical to that obtained[18] with *in situ* Pr-doped GaN, thus establishing the feasibility of FIB direct-write with Pr for GaN ELD fabrication. Recently, visible red emission was similarly achieved using conventional ion implantation of Pr^+ into GaN films grown by metal-organic chemical vapor deposition.[34]

The third primary color (blue) was achieved[20] by doping GaN with thulium.

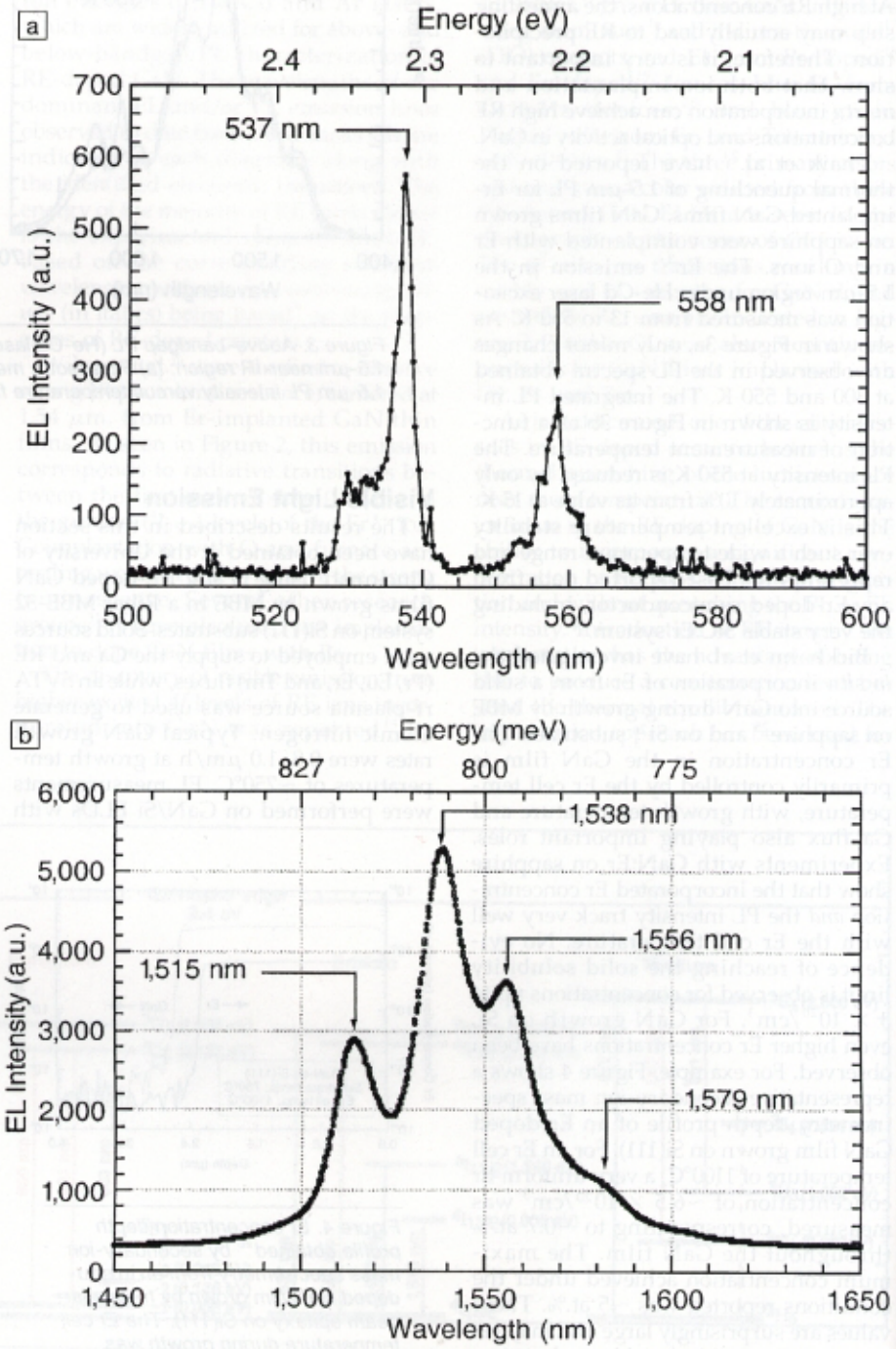

Figure 5. Er-activated emission spectra from indium tin oxide/GaN:Er light-emitting devices (LEDs):[17] (a) visible emission in the green (bias current of 4.4 mA), and (b) near-IR emission at ~1.5 μm (bias current of 8.12 mA).

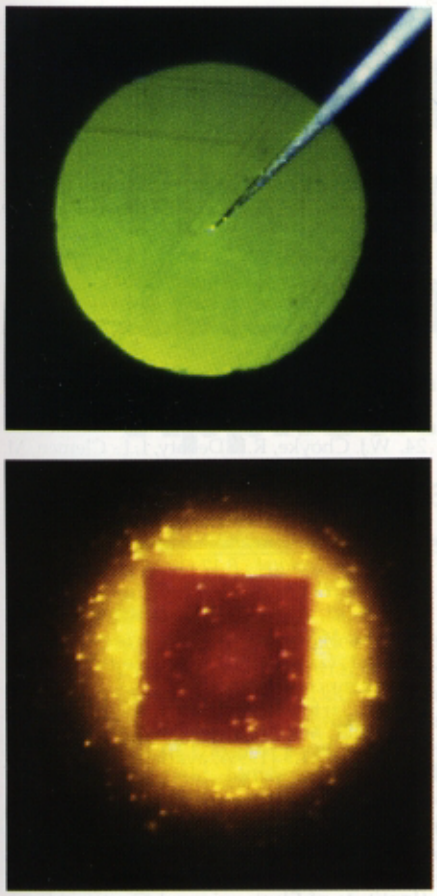

Figure 6. Photographs of visible emission from RE-doped GaN. (a) Green EL from in situ-doped GaN:Er LED.[17] The diameter of the emitting area is 4 mm; the probe tip is seen making contact with the center of the ITO electrode. (b) Red PL from Pr focused-ion-beam-implanted GaN.[25] Implanted area is 141 μm × 141 μm square.

Intense blue emission is visible at room temperature from ITO/GaN:Tm ELDs. The main emission peak is at 477 nm, corresponding to the $^1G_4 \rightarrow {}^3H_6$ transitions of the Tm^{3+} ion. As shown in Figure 2, additional emission lines are observed at 647 and 801 nm, corresponding to the $^1G_4 \rightarrow {}^3H_4$ and $^1G_4 \rightarrow {}^3H_5$ transitions, respectively. If two or more RE elements incorporated into GaN emit in the visible simultaneously, the human eye would perceive an additive mixture of the colors. It should be possible to adjust the relative concentrations of the RE dopants in GaN, and hence the intensities of the corresponding wavelengths, so that the mixture would produce any color throughout the visible spectrum. In addition, with proper masking, it could be possible to achieve a full-color display with separately biased red-, green-, and blue-emitting regions on a single substrate and in a single plane. The first such color mixing in RE-doped GaN was achieved using a combination of Er and Tm. The visible EL spectrum[21] from an ITO/GaN ELD codoped during growth with Er and Tm is shown in Figure 7. Both the Tm blue emission at 478 nm and the Er green emissions at 537 and 558 nm are present. This blue/green combination results in the overall color of aqua or turquoise, as seen in the Er + Tm GaN ELD shown on the cover of this issue.

The potential impact of RE-doped GaN on display technology can be evaluated with the aid of a chromaticity diagram, which displays the relationship between the color hues distinguished by the human eye and the three primary colors. Figure 8 contains the uniform chromaticity diagram (UCD) revised in 1976 by the Commission Internationale de l'Eclairage (CIE). Briefly, the CIE diagram utilizes the fact that for any hue, the combined percentage of the three primary colors is 100%. Therefore, the percentages of only two of the three

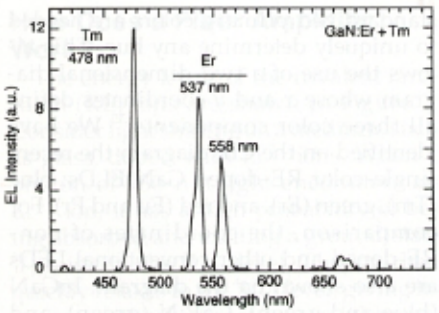

Figure 7. Visible EL spectrum from an ITO/GaN LED codoped during growth[21] with Er and Tm. Both the Tm blue emission at 478 nm and the Er green emissions at 537 and 558 nm are present, resulting in the overall color of aqua or turquoise. Bias current is 2.72 mA.

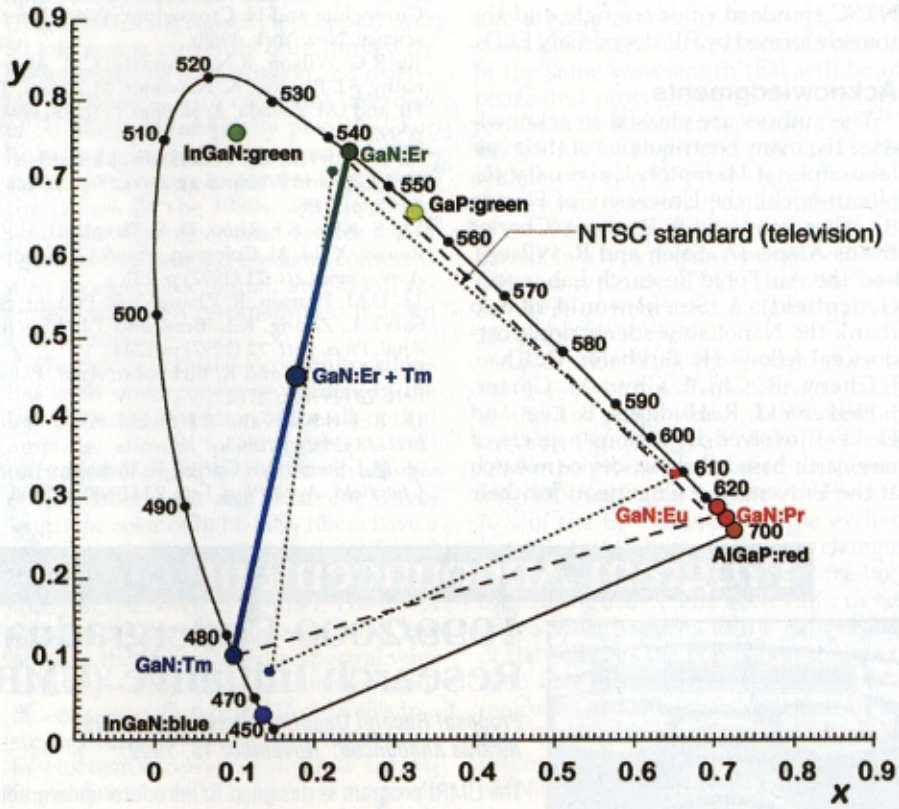

Figure 8. The Commission Internationale de l'Eclairage (CIE) chromaticity diagram showing the locations of RE-activated GaN LEDs: GaN:Tm for blue emission, GaN:Er for green emission, and GaN:Eu and GaN:Pr for red emission. Mixed colors can be produced by combining the appropriate RE dopants, as in the case of GaN codoped with Er and Tm producing the aqua color emission. NTSC is the U.S. National Television System Committee.

standardized primary colors are needed to uniquely determine any hue. This allows the use of a two-dimensional diagram whose x and y coordinates define all three color components.[35] We have identified on the CIE diagram the recent single-color RE-doped GaN ELDs: blue (Tm), green (Er), and red (Eu and Pr). For comparison, the coordinates of non-RE-doped and other conventional LEDs are also shown on the diagram: InGaN (blue and green), GaP:N (green), and AlGaP (red). For the mixed color of the GaN:(Er + Tm) devices, we estimate the UCD coordinates as $x = 0.18$ and $y = 0.45$, placing the color approximately halfway on the line between the Tm and Er devices. We expect that combinations of RE dopants in various ratios will produce a multitude of hues within the GaN:RE triangle. Also shown on the CIE diagram are the three primary colors adopted by the U.S. Federal Communications Commission, based on the recommendation of the U.S. National Television System Committee (NTSC) as standards for color television. It is very promising to note the excellent overlap between the NTSC standard color triangle and the triangle formed by RE-doped GaN ELDs.

Acknowledgments

The authors are pleased to acknowledge the many contributions of their collaborators at Hampton University (U. Hömmerich), the University of Florida (C. Abernathy and S. Pearton), Charles Evans Assoc. (A. Saleh and R. Wilson), and the Air Force Research Laboratory (J. Scofield). A. Steckl would like to thank the NanoLab students and postdoctoral fellows (R. Birkhahn, D. Chao, J. Cheng, R. Chi, I. Chyr, M. Garter, J. Heikenfeld, R. Hudgins, B. Lee, and D. Lee) involved in various aspects of rare-earth-based photonic-device research at the University of Cincinnati for their enthusiasm, creativity, and hard work. The research at Cincinnati was partially sponsored by the U.S. Army Research Office/Ballistic Missile Defense Organization, MRL-Department of Defense, and the National Science Foundation.

References

1. S. Coffa, G. Franzò, and F. Priolo, *MRS Bull.* **23** (4) (1998) p. 25.
2. P.N. Favennec, H. L'Haridon, M. Salvi, D. Moutonnet, and Y. Le Guillou, *Electron. Lett.* **25** (1989) p. 718.
3. M. Neuberger, *II-VI Ternary Compound Data Tables*, EPIC-S-15 (Electronic Properties Information Center, Hughes Aircraft, Culver City, CA, 1972).
4. O. Madelung, *Semiconductors, Group IV Elements and III-V Compounds* (Springer-Verlag, Berlin, 1991).
5. O. Madelung, *Semiconductors, Basic Data*, 2nd ed. (Springer-Verlag, Berlin, 1996).
6. J.M. Zavada and D. Zhang, *Solid-State Electron.* **38** (1995) p. 1285.
7. S. Nakamura and G. Fasol, *The Blue Laser Diode* (Springer-Verlag, Berlin, 1997).
8. H. Morkoç, *Nitride Semiconductors and Devices* (Springer-Verlag, Berlin, 1999) in press.
9. G.H. Dieke, *Spectra and Energy Levels of Rare Earth Ions in Crystals*, edited by H.M. Crosswhite and H. Crosswhite (Wiley Interscience, New York, 1968).
10. R.G. Wilson, R.N. Schwartz, C.R. Abernathy, S.J. Pearton, N. Newman, M. Rubin, T. Fu, and J.M. Zavada, *Appl. Phys. Lett.* **65** (1994) p. 992.
11. J.T. Torvik, R.J. Feuerstein, J.I. Pankove, C.H. Qiu, and F. Namavar, *Appl. Phys. Lett.* **69** (1996) p. 2098.
12. S. Kim, S.J. Rhee, D.A. Turnbull, E.E. Reuter, X. Li, J.J. Coleman, and S.G. Bishop, *Appl. Phys. Lett.* **71** (1997) p. 231.
13. D.M. Hansen, R. Zhang, N.R. Perkins, S. Safvi, L. Zhang, K.L. Bray, and T.F. Kuech, *Appl. Phys. Lett.* **72** (1997) p. 1244.
14. A.J. Steckl and R. Birkhahn, *Appl. Phys. Lett.* **73** (1998) p. 1702.
15. R. Birkhahn and A.J. Steckl, *Appl. Phys. Lett.* **73** (1998) p. 2143.
16. A.J. Steckl, M. Garter, R. Birkhahn, and J. Scofield, *Appl. Phys. Lett.* **73** (1998) p. 2450.
17. M. Garter, J. Scofield, R. Birkhahn, and A.J. Steckl, *Appl. Phys. Lett.* **74** (1999) p. 182.
18. R. Birkhahn, M. Garter, and A.J. Steckl, *Appl. Phys. Lett.* **74** (1999) p. 2161.
19. J. Heikenfeld, M. Garter, D.S. Lee, R. Birkhahn, and A.J. Steckl, *Appl. Phys. Lett.* **75** (9) (1999) p. 1189.
20. A.J. Steckl, M. Garter, D.S. Lee, J. Heikenfeld, and R. Birkhahn, *Appl. Phys. Lett.* **75** (15) (1999).
21. R. Birkhahn, M. Garter, J. Heikenfeld, D.S. Lee, and A.J. Steckl (unpublished).
22. H. Lozykowski, W.M. Jadwisienczack, and I.M. Brown, *Appl. Phys. Lett.* **74** (8) (1999) p. 1129.
23. M. Thaik, U. Hömmerich, R.N. Schwartz, R.G. Wilson, and J.M. Zavada, *Appl. Phys. Lett.* **71** (1997) p. 2641.
24. W.J. Choyke, R.P. Devaty, L.L. Clemen, M. Yoganathan, G. Pensl, and Ch. Hassler, *Appl. Phys. Lett.* **65** (1994) p. 1668.
25. R. Birkhahn, R. Hudgins, D.S. Lee, A.J. Steckl, R.J. Molnar, A. Saleh, and J.M. Zavada *J. Vac. Sci. Technol., B* **17** (1999) p. 1195.
26. R. Birkhahn, R. Hudgins, D.S. Lee, A.J. Steckl, A. Saleh, R.G. Wilson, and J.M. Zavada, *MRS Internet J. Nitride Semicond. Res.* **4S1**, G3.80 (1999), available from http://nsr.mij.mrs.org/2/5/.
27. M. Garter, R. Birkhahn, A.J. Steckl, and J. Scofield, *MRS Internet J. Nitride Semicond. Res.* **4S1**, G11.3 (1999), available from http://nsr.mij.mrs.org/2/5/.
28. S. Nakamura, M. Senoh, N. Iwasa, and S. Nagahama, *Jpn. J. Appl. Phys.* **34** (1995) p. L797.
29. A.J. Steckl, in *Proc. Advanced Workshop on Frontiers in Electronics* cat. No. 97TH8292 (Institute of Electronic and Electrical Engineering, Piscataway, NJ, 1997) p. 47.
30. A.J. Steckl and I. Chyr, *J. Vac. Sci. Technol., B* **17** (1999) p. 362.
31. L.C. Chao and A.J. Steckl, *J. Vac. Sci. Technol., B* **17** (1999) p. 1051.
32. L.C. Chao and A.J. Steckl (unpublished).
33. L.C. Chao and A.J. Steckl, *Appl. Phys. Lett.* **74** (1999) p. 2364.
34. J.M. Zavada, R.A. Mair, C.J. Ellis, J.Y. Lin, H.X. Jiang, R.G. Wilson, P.A. Grudowski, and R.D. Dupuis, *Appl. Phys. Lett.* **75** (1999) p. 790.
35. R.W.G. Hunt, *Measuring Color*, 2nd ed. (Ellis Harwood, UK, 1991). □